J Mol Model (2004) 10:216–222
DOI 10.1007/s00894-004-0191-z

ORIGINAL PAPER

Daxiong Han · Haiyan Wang · Nailin Ren

Molecular modeling of B-DNA site recognition by Ru intercalators: molecular shape selection

Received: 3 November 2003 / Accepted: 2 March 2004 / Published online: 1 May 2004

Abstract In this work, molecular modeling methods have been applied to the interaction characterization of polypyridyl transitional-metal complexes with the oligonucleotide (B-DNA fragment). In order to explore the factors governing the groove recognition and intercalative depth, we establish a simple and practical docking method (step-by-step docking operation) to obtain potential curves while making complexes inset into B-DNA along an assigned path. Energy values in the potential curve are obtained from energy minimization of binding geometries. Modeling results clearly show that the optimum binding conformation corresponding to the global minimum in the potential curve for each complex is found to correlate well with the experimental results. Our results also confirm that minor changes of the ligand structure can lead to profound influences on binding geometries, so the molecular shape of the complexes is a predominant factor in governing the binding mode. Moreover, we find that the vdW force and "water molecular effect" are strongly associated with molecular-shape selection in our model. These results complement and extend the knowledge of the nature of these complexes binding to B-DNA.

Keywords MM+ force field · Docking · B-DNA · Metal complex

Introduction

There is substantial interest in delineating those factors that contribute to B-DNA-site recognition by polypyridyl transitional-metal complexes [1, 2, 3, 4, 5, 6, 7]. Despite a considerable amount of published material, the detailed structural information on the nature of the binding interaction has remained relatively modest. For example, $[Rh(phen)_2phi]^{3+}$ associates with DNA in the major groove through intercalation; however, $[Ru(phen)_2dpq]^{2+}$, similar to $[Rh(phen)_2phi]^{3+}$, prefers to bind to DNA in the minor groove; for $[Ru(phen)_2dppz]^{2+}$, the classical intercalative mode has been accepted by most scientists, but there is still intense controversy on binding to DNA from the major or minor grooves [8, 9]. Many experimental observations have shown that different binding modes (intercalative orientation and depth) for this sort complex occur because of the steric structural difference. Thus, how ligands with varied bulk influence the binding interaction is an interesting subject. However, it is difficult to investigate through experimental methods because different complexes are frequently not reported in the same piece of work and are not easy to extract from the literature. Therefore, in order to carry out a systematic study of the interaction between Ru(Rh) complexes and DNA, we have compared a set of binding geometries of complexes from molecular mechanics calculations. The complexes (only Δ-isomers) with primary structure properties in our study are shown in Fig. 1. Using the manual docking methodology [10, 11], we obtain potential curves

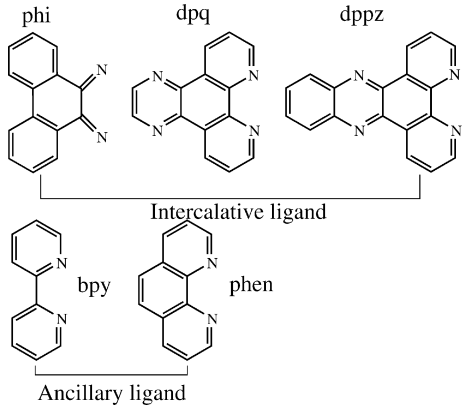

Fig. 1 Intercalative ligand and ancillary ligand of $[Ru(phen)_2dpq]^{2+}$, $[Ru(phen)_2dppz]^{2+}$, $[Ru(bpy)_2dppz]^{2+}$, $[Rh(phen)_2phi]^{3+}$, $[Rh(bpy)_2phi]^{3+}$

D. Han · H. Wang · N. Ren (✉)
Department of Chemistry,
Hanshan Teachers College,
52/1041 Chaozhou, China
e-mail: hsrnl@163.com
Tel.: +86-351-4120789

Table 1 Metal complex parameters for the MM+ force field

Atom types	Parameters[a]
N–Ru(Rh)	2.6837 mdyn Å^{-1} (kr) 2.056 Å (l_0)[b]
	2.6941 mdyn Å^{-1} (bond moment)
N–Ru(Rh)–N	0.1760 mdyn Å rad^{-2} (k_b)
	180.0000 deg (θ_0)
C–N–Ru(Rh)	0.7195 mdyn Å rad^{-2} (k_b)
	123.5054 deg (θ_0)
Ru	2.34 Å (van der Waals r)
	0.438 kcal mol^{-1} (ϵ)
Rh	2.71 Å (van der Waals r)[c]

[a] From [25] and refined
[b] From [18]
[c] From Chem3D program package

for complexes that insert into the major or minor grooves of B-DNA along an assigned path. For each complex, the optimum binding geometry is regarded as occurring at the global minimum of the potential curve. Through detailed analyses of the intercalative ligand and ancillary ligand effects on binding geometries, the vdW (van der Waals) forces and "water molecule effect" in the microscopic-environment effects on composite poten-tials, we have explored how the molecular shape governs the complexes to B-DNA-site recognition, i.e. molecular shape selection, and developed a detailed structural understanding of how these complexes interact with the B-DNA helix.

Computational method

With appropriate parameters, molecular mechanics methods are useful in elucidating the structure of metal-containing molecules. The MM+ force field in the HyperChem 6.0 program package is one of the most accurate force fields widely used for calculations of "small" molecules [12]. MM+ was not originally parameterized for Ru and Rh ions. After adding the same parameters for them except the van der Waals radius (Table 1), we find that MM+ can treat metal complexes as it would treat any other molecular. The starting geometry of the complexes is fully set up in D_3 symmetry. Geometry optimization is performed using a conjugate-gradient procedure with a convergence criterion of 0.01 kcal mol^{-1} Å^{-1}.

The simulation of complexes bound to the B-DNA minor or major grooves is carried out using a step-by-step docking operation. Firstly, the crystallographic structure of the B-DNA fragment d(CGCAATTGCG)$_2$ was retrieved from the Brookhaven Protein Database (ID: 252D). The crystallographic water molecules were deleted, and energy minimization performed. It has been shown that the complexes bind relatively unspecifically to B-DNA with a slight preference for AT-rich regions [13, 14, 15], so we selected insertion of the complexes into the A_5T_6/T_6A_5 base step of the B-DNA fragment in a "head-on" fashion [16], see Scheme 1. The *dpq* twofold axis is perpendicular to both the base-pairs' long axis and the helical axis. While the complex atom positions were fixed, the rest are minimized to allow the free B-DNA to adjust to accommodate the complex suitably, and subsequently the whole system is minimized without any restraints by the Polak–Ribiere conjugate method with a convergence criterion of 0.5 kcal mol^{-1} Å^{-1} in vacuum. While manually changing the intercalative depth of the complex, the binding structures along the designed pathway are constructed individually, and then independently minimized to obtain energy values as potential curves (energy versus intercalative depth). Here, intercalative depth is defined as the distance from the Ru(Rh) atom to the cross point between the twofold axis and the helical axis.

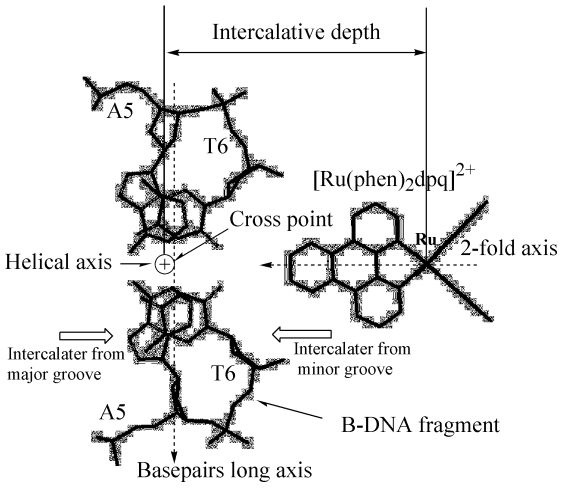

Scheme 1 Schematic illustration of the complexes intercalated into the B-DNA fragment

In order to explore the "water-molecule effect" in the intercalation process of the complexes, the same bulk (40 Å, 25 Å and 40 Å) of *TIP3P* water boxes hydrate each composite minimized above in vacuum. In the composites, intercalative depth and orientation of complex are different. Keeping all atoms of the composite at fixed positions, energy minimization of the water molecules is carried out to adjust their orientations, and subsequently the whole box system is minimized. Finally, the optimum conformation of the composites (i.e. the best relative position of each complex bound to the B-DNA) is found by analyzing the potential curves in water solvent. All calculations are performed on a 2.4-GHz PC using the MM+ force field in HyperChem 6.0, using default settings consistently (assigning a dielectric of 1.0).

Results and discussion

Metal complexes

In our model, the entire complex is treated as a covalently bound entity, using standard stretching and bending potentials to describe intramolecular interactions, so the parameters have a significant effect on the ability of the force field to reproduce the complex structure to a satisfactory level of precision [17]. Therefore, we selected the Ru (Rh) parameters from the literature to match the

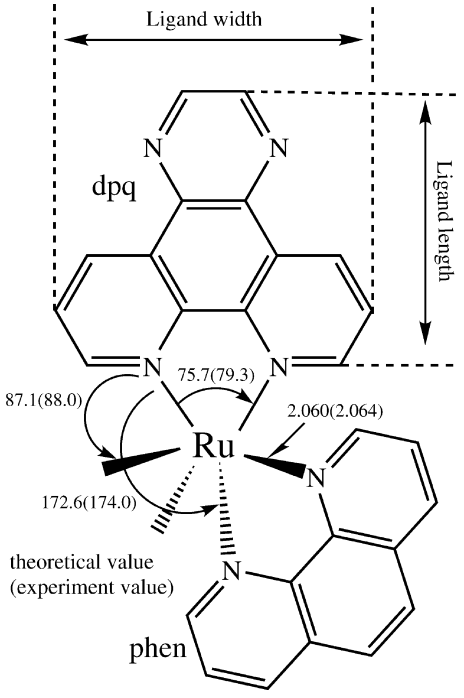

Fig. 2 Comparison of the theoretical and experiment values of the $[Ru(phen)_2dpq]^{2+}$ structure

functional formalism of MM+ (Table 1). As an illustrative example of the accuracy of the present parameters, the structural data of $[Ru(phen)_2dpq]^{2+}$ obtained from the MM+ calculation are compared with the reported X-ray structure [18], as shown in Fig. 2. The difference between theoretical and experimental values for the $[Ru(phen)_2dpq]^{2+}$ is within 0.005 Å for bond length and within better than 4° for bond angles. These results indicate that the parameters for Ru (Rh) used in our recent work are indeed very accurate.

Binding simulation in vacuum

The complexes were docked manually from 18 Å to 4.5 Å at about 1-Å intervals. The H-bonds between nucleobases are basically maintained in the intercalative process of complexes. The binding potential curves of five different complexes are clearly different in Fig. 3. The reason for the difference may stem from two aspects, including both intercalative ligands and ancillary ligands.

Intercalative ligand effect

The shape and bulk of the intercalative ligand provide a primarily structural element in dominating the binding mode of the complexes. This is indicated strongly by the fact that the overall curve trends of the same intercalative ligand show high similarities, even when the ancillary ligands are not identical (see b and c, d and e in Fig. 3). If intercalative ligand insertion into the basepairs region is

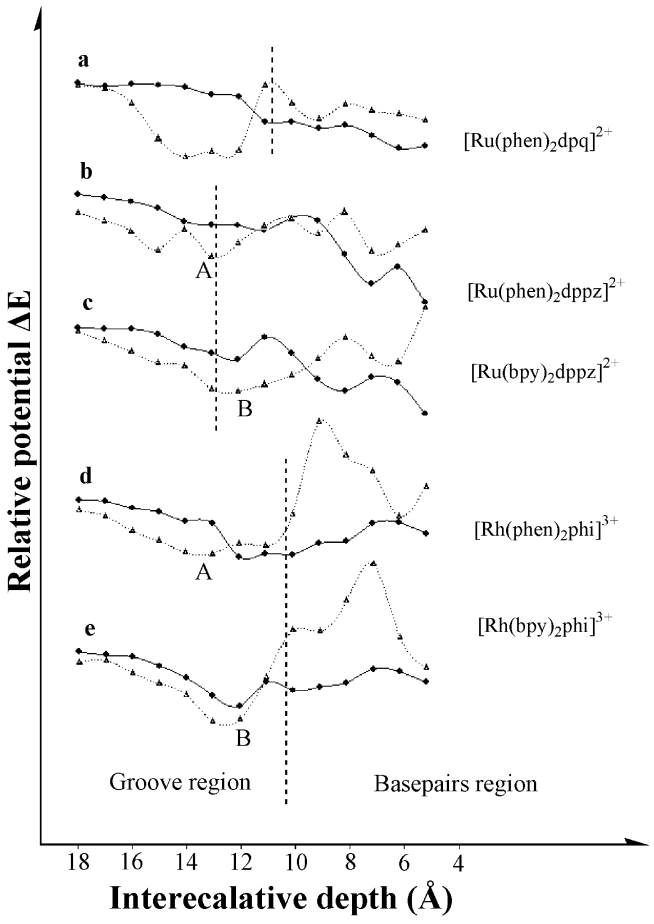

Fig. 3 Relative potential curves for the five complexes binding B-DNA in vacuum. The *heavy line* shows major-groove intercalation; the *dashed line* is for the minor groove. The starting energy value of the minor groove is regarded as the reference value

regarded as the intercalation mode (in contrast to the groove-binding mode), the modeling results show that increasing the length of the intercalative ligand is more favorable for the intercalative mode. For *dpq* and *phi* complexes, the global minima all occur in the groove region. Comparatively, the global minima of *dppz* complexes occur in the basepairs region. The reason is easily understood. The shorter intercalative ligand stacking with basepairs will of necessity make two ancillary ligands close to the B-DNA backbone, further leading to vdW repulsion. In contrast, the longer *dppz* not only increases the amount of direct overlap between the intercalative ligand and the bases, but also puts the ancillary *phen* (or *bpy*) further away from the groove bottoms of the B-DNA to avoid steric shielding. Thus, the *dppz* can insert deeply into the base stack. On the basis of the above analysis, we suggest that the length of the intercalative ligand is a primary factor for the intercalation mode selected.

Structurally, the width of the intercalative ligand provides another constraint and selection for the binding mode, such as groove selection. When the *phi* inserts into the basepairs region from the minor groove, the potential

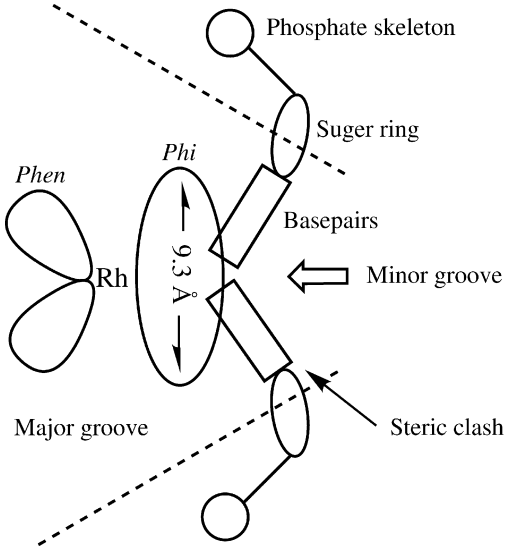

Scheme 2 Schematic representation of a base pair fragment with a *phi* complex intercalated from the major groove

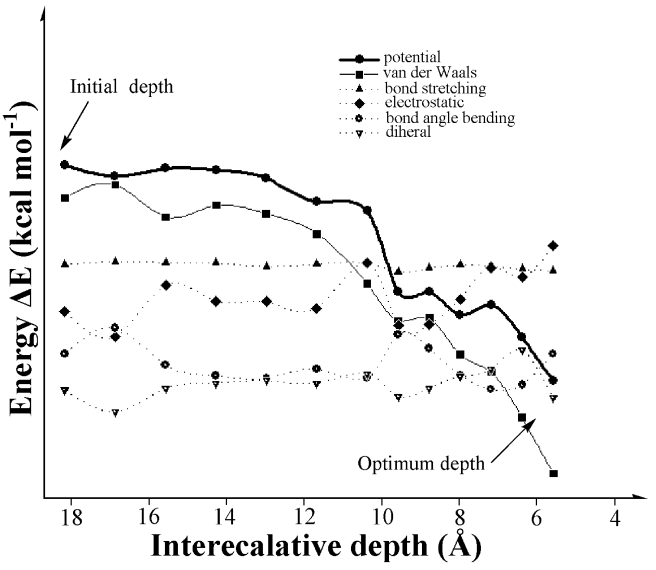

Fig. 4 The change trend of several energetic terms for [Ru(phen)$_2$dpq]$^{2+}$ binding system in vacuum

profiles for [Rh(phen)$_2$phi]$^{3+}$ and [Rh(bpy)$_2$phi]$^{3+}$ are uphill with a "peak", which shows an obvious difference to other profiles (see d and e in Fig. 3). Due to the use of imines as coordinating chelators, the *phi* has an expanse of aromatic structure along the basepairs' long axis so as to form a broad head. The shape of a B-DNA intercalation site, though flexible, is distinctly trapezoidal, with its widest edge on the major groove side (Scheme 2). This shape, combined with the bottom widths of the B-DNA minor groove (9.2 Å) and the head width (9.3 Å) of the *phi*, support the conclusion that B-DNA binding for the *phi* complexes must occur from the major groove. In this orientation, the steric overlap between the overhanging H atom of the *phi* and either O atom (the ribose ring oxygen) or H atom on the other side of the intercalation site shown through the "peak" in the potential curve is avoided, and the extended orientation of the nucleobases facing the major groove also allows significant aromatic–aromatic overlap.

Ancillary ligand effect

Firstly, ancillary ligands are brought into position against the B-DNA phosphate skeleton and basepairs, and as a result the intercalative depth of complexes will be affected by ancillary ligands. For example, when the surface area of ancillary ligands *(phen>bpy*) decreases, the point A, a local minimum in the potential profiles of minor groove, moves right to point B (see b, c and d, e profiles in Fig. 3). The phenomenon shows clearly that the complexes with smaller ancillary ligands intercalate deeper. Secondly, Fig. 3 shows that, for the five complexes, the relative potential of the minor groove is always lower than that of the major groove in the groove region. This is explained by the fact that the vdW fit between B-DNA and ancillary ligands is substantially better in the minor-groove orientation, i.e. the distance between C atoms of B-DNA and C atoms of ligands is not too close so as to provide a steric blockade, but sufficiently close to allow a stabilizing vdW contact. Graphic measurement results show that the widths of the minor and major grooves are about 10.0 Å and 17.0 Å respectively, and the widths of the complexes are about 6.8 Å. In this model the C–C nonbonded distance is about 4.0 Å. Therefore, a favorable nonbonded contact (10 Å–6.8 Å=3.2 Å) will only be available binding from the minor groove.

Intrinsic force

The above discussion reveals that the entire molecular shape is a significant factor governing the site selection. Thus, what is an intrinsic force to be associated with molecular shape selection? By delineating the changes of mainly energetic terms for the [Ru(phen)$_2$dpq]$^{2+}$ intercalation from the minor groove, it is clearly observed that the descending trend of potential is only consistent with that of vdW energy under the simulation conditions of our study (Fig. 4). No matter what binding mode the five complexes adopt, the characteristic occurs in general in downhill potential profiles. By this token, vdW forces play a major role in stabilizing the composite. In other words, only when the complex shape fits the B-DNA helix in the intercalation site well enough, does the binding produce vdW attraction, which makes the system potential drop substantially. Therefore, it is reasonable to deduce that vdW forces are an intrinsic force for site specificity dominated by molecular shape.

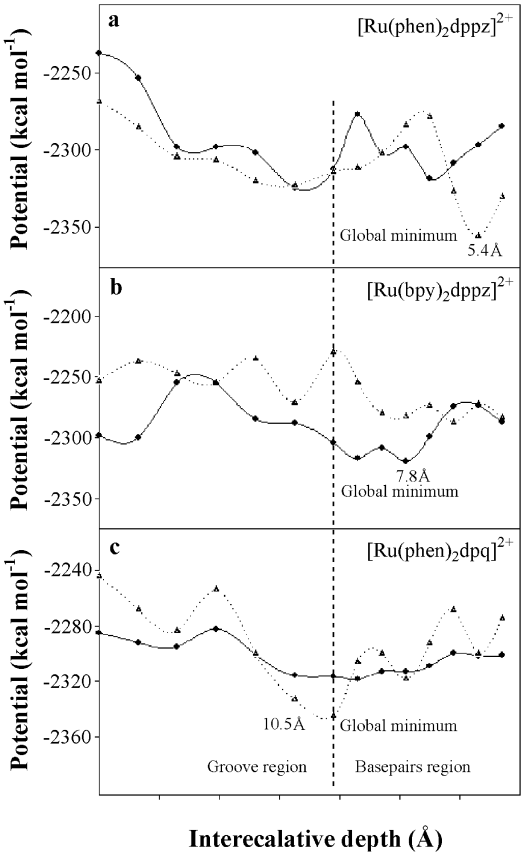

Fig. 5 Potential curves for **a** $[Ru(phen)_2dppz]^{2+}$, **b** $[Ru(bpy)_2dppz]^{2+}$ and **c** $[Ru(phen)_2dpq]^{2+}$ binding in a water environment. The *heavy line* shows major-groove intercalation; the *dashed line* is for the minor groove

Binding simulation in water environment

The potential curves in the water environment show that the molecular shape is still the main factor dominating the binding mode based upon the following two aspects.

Groove selection

There are still divergences about intercalative orientations of *dppz* complexes from experimental data. Among all sorts of viewpoints Barton's and Norden's are the most representative. Barton suggested that the intercalation occurs from the major groove [19]. In contrast, Norden proposed that this sort complex binds to B-DNA from the minor groove [20, 21]. Here, the intercalative orientation will in theory be explored according to potential curves, in which the global minimum corresponds to the optimum binding structure. For $[Ru(phen)_2dppz]^{2+}$, the global minimum does occur in the minor groove with a deep valley (Fig. 5a), and a minor-groove intercalative fashion is adopted. The lateral view of its optimum binding conformation (Scheme 3) shows that the ancillary *phens* are located in the minor groove together with the terminal ring of the *dppz* projecting out into the major groove and

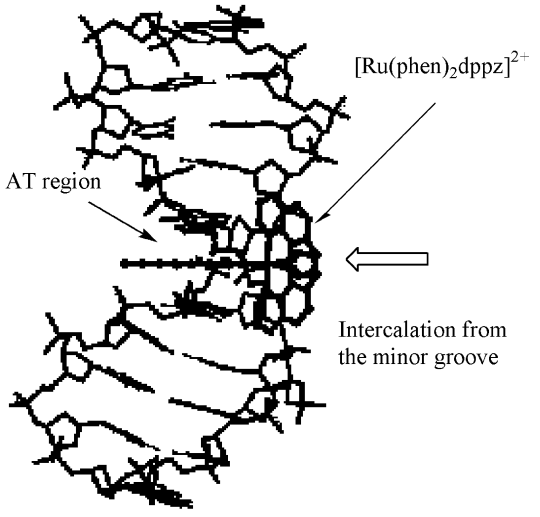

Scheme 3 The lateral view of the optimum binding conformation for the $[Ru(phen)_2dppz]^{2+}$

the adjacent basepairs fully separated. However, Fig. 5b shows that the major-groove potential is generally lower than that of the minor-groove, so $[Ru(bpy)_2dppz]^{2+}$ is a classical intercalator of major-groove binding. The $[Ru(bpy)_2dppz]^{2+}$ differs from $[Ru(phen)_2dppz]^{2+}$ only by removing the protruding –CH–CH– group of the ancillary *phen* moiety, which makes their binding modes distinctly different in a water environment. Thus, it can be seen that the binding model of the *dppz* complexes is sensitive to the change of molecular shape. How does the complex shape affect the binding? Through observing modeling graphics we find that the shape-match difference between *phen* and *bpy* with the B-DNA brings about the marked differences in the number and distribution of water molecules in the fixed box. Because the interaction of water molecules is the main contribution to the decreasing potential values of the box system in our model, a small change of the water system will lead to an obvious change of potential value, thereby affecting the binding mode selected. Considering that the binding model of the *dppz* complexes is uncertain in experimental studies, we infer that the *dppz* complexes may adopt multi-binding modes based upon the ancillary ligands and DNA sequence differences. In addition, the optimum intercalative depths for $[Ru(phen)_2dppz]^{2+}$ and $[Ru(bpy)_2dppz]^{2+}$ are different (5.4 Å and 7.8 Å, respectively). The reason is that for $[Ru(bpy)_2dppz]^{2+}$, the intercalative orientation of the *dppz* is not in accord with the extending orientation of basepairs, thereby producing strong vdW repulsions (see Scheme 2). Similar to $[Ru(phen)_2dppz]^{2+}$, $[Ru(phen)_2dpq]^{2+}$ also prefers to bind B-DNA in the minor groove based on potential calculations (Fig. 5c), in good qualitative agreement with Collins's experiment result [22]. Its intercalative depth (10.5 Å) is much smaller due to the shorter intercalative ligand *dpq*. The edge of the *dpq* is only coplanar with the basepairs, but does not open the basepairs' stack, and accordingly suggests that groove-binding fashion or "partially inserted" modes from the minor groove are possible.

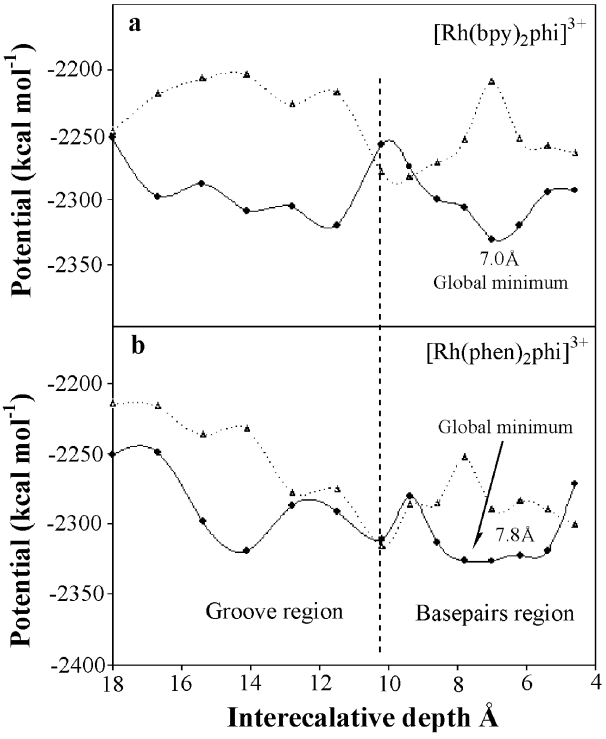

Fig. 6 Potential energy curves for $[Rh(bpy)_2phi]^{3+}$ and $[Rh(phen)_2phi]^{3+}$ binding in a water environment. The nature of the lines is the same as in Fig. 5

For $[Rh(bpy)_2phi]^{3+}$ and $[Rh(phen)_2phi]^{3+}$, the major binding orientation can be revealed clearly by the potential curves in Fig. 6: the major-groove potential is considerably lower in most sites and the potential profiles only cross partly in the boundary between the basepairs region and the groove region. NMR studies indicated that the *phi* complexes intercalate only from the major groove [23, 24]. The consistency of molecular modeling and experimental results confirm the feasibility of our modeling protocol. Moreover, the water environment simulated by *TIP3P* water molecules makes the binding modes more reasonable for reproducing the NMR deduction: the *phi* ligand produces sufficient stacking interactions with the nucelobases in the major groove orientation. Potential profiles show that their optimum intercalative depth changes from about 12.0 Å in vacuum to about 7.0–7.8 Å in water (see Fig. 3 and Fig. 6, respectively). This is explained by the fact that for the water box with free water molecules, the complexes approaching the groove bottom of B-DNA will vacate space to accommodate more water molecules. An increase in water molecules will make the potential rapidly descend, while there is no such water effect in vacuum.

In the case of the five complexes, the relation of molecular shape and groove selection is evident: (1) geometric characters (long and thin) for the intercalative ligand such as *dppz* are favorable for the minor-groove intercalative fashion; (2) the *phi* complexes with broad heads bind only from the major groove; (3) the ancillary *phen* may be favorable for the complex bound in the minor groove.

Water-molecule effect

The water environment is simulated with a fixed water box, where the number of water molecules is associated with the binding conformation. The above results show that the binding modes obtained by simulations are basically identical with those provided by experiments. This implies that the water microheterogeneity in number and orientation may better embody the effect of water molecules on the complexes' binding. The water number depends on intercalative depth, molecular bulk and groove selection (Table 2). For $[Ru(bpy)_2dppz]^{2+}$, $[Rh(phen)_2phi]^{3+}$ and $[Rh(bpy)_2phi]^{3+}$ the mean number of water molecules in the major groove is larger than that in the minor groove (997>990, 998>989, 1000>989), in contrast

Table 2 The dependence of the water number in the fixed box on the intercalative depth

Depth (Å)	$[Ru(phen)_2dpq]^{2+}$		$[Ru(phen)_2dppz]^{2+}$		$[Ru(bpy)_2dppz]^{2+}$		$[Rh(phen)_2phi]^{3+}$		$[Rh(bpy)_2phi]^{3+}$	
	Minor groove	Major groove	Minor groove	Major groove	Minor groove	Major groove	Minor groove	Major groove	Minor groove	Major groove
18.0	984	991	991	978	981	1001	977	994	980	993
16.7	989	990	994	987	985	995	976	992	981	998
15.4	985	991	988	993	987	988	976	992	977	992
14.1	989	1001	996	992	983	995	980	991	978	1002
12.8	994	993	1000	991	980	993	983	993	984	999
11.5	1006	997	1003	993	988	992	983	997	982	1006
10.2	1008	994	1003	991	990	996	1001	997	992	993
9.4	1000	996	1002	990	991	1005	999	993	1002	997
8.6	1000	1002	990	999	1002	996	998	997	1003	1003
7.8	1001	996	996	997	998	998	991	1001	998	1005
7.0	998	1002	996	1000	990	1000	1004	1007	989	1006
6.2	994	999	1001	997	993	997	993	1006	992	1009
5.4	992	1000	1004	999	996	998	995	1006	998	1004
4.6	997	995	1007	994	998	1000	998	1001	994	999
Mean number	995	996	998	993	990	997	989	998	989	1000

to the $[Ru(phen)_2dppz]^{2+}$, the mean value in the minor groove is larger (998>993). These sequences correspond completely to their optimum binding orientation. Moreover, the optimum intercalative depths for every complex occur at the maximum water-number region (see bold text in Table 2). These features strongly indicate that the better the fit between complex and intercalative site, the more room for water molecules and the lower potential afforded by water interaction. Hence, it may be said that the action of molecular shape governing the binding mode is repeated in the "water-molecule effect".

Conclusions

Through the use of molecular modeling, this work has characterized the structural details of the interactions of polypyridyl Ru(Rh) intercalators with the B-DNA oligonucleotide. First, optimum binding modes of the five complexes have been obtained, and these modes correspond well to the experimental results. Second, these complexes are found to display vastly different binding modes because of subtle differences in their individual shapes, which suggests that this sort of metal complexes might serve to recognize DNA sites based upon matching shape. More importantly, we have further illustrated that changes in the ligand architecture will lead to profound influences on binding geometries mainly from both vdW force changes and the "water-molecule effect". In short, this modeling work will increase an understanding of the complexes' binding to the helix. It will be important to make the octahedral metalointercalaters become useful in biological applications and assays.

Acknowledgments The authors acknowledge the support of Provincial Education Science Foundation of GuangDong (Series Number: 0164).

References

1. Sitlani A, Long EC, Pyle AM, Barton JK (1992) J Am Chem Soc 114:2303–2312
2. Arounaguiri S, Maiya BG (1996) Inorg Chem 35:4267–4270
3. Lincoln P, Norden B (1998) J Phys Chem B 102:9583–9594
4. Terbrueggen RH, Johann TW, Barton JK (1998) Inorg Chem 37:6874–6883
5. Holmlin RE, Yao JA, Barton JK (1999) Inorg Chem 38:174–189
6. Patterson BT, Collins JG, Foley FM, Keene FR (2002) J Chem Soc Dalton Trans 4343–4350
7. Wilhelmsson LM, Esbjo1rner EK, Westerlund F, Norden B, Lincoln P (2003) J Phys Chem B 107:11784–11793
8. Holmlin RE, Steamp EDA, Barton JK (1998) Inorg Chem 37:29–34
9. Tuite E, Lincoln P, Norden B (1997) J Am Chem Soc 119:239–240
10. Han DX, Yang P (2000) Sci Chin B 43:516–523
11. Yang P, Han DX, Xiong ZH (2001) J Mol Struct (Theochem) 540:211–219
12. HyperChem, Release 6.0 (2000) Hypercube Inc
13. Lane AN, Jenkins TC, Brown T, Neidle S (1991) Biochemistry 30:1372–1385
14. Watts CR, Kerwin SM, Kenyon GL, Kuntz ID, Kallick DA (1995) J Am Chem Soc 117:9941–9950
15. Frankjin CA, Fry JV, Collins JG (1996) Inorg Chem 35:7541–7545
16. Dupureur CM, Barton JK (1997) Inorg Chem 36:33–43
17. Marques HM, Warden C, Monye M, Shongwe MS, Brown KL (1998) Inorg Chem 37:2578–2581
18. Collins JG, Sleeman AD, Janice RAW, Greguric I, Hambley TW (1998) Inorg Chem 37:3133–3141
19. Erkkila KE, Odom DT, Barton JK (1999) Chem Rev 99:2777–2795
20. Ihtshamul H, Lincoln P, Suh D, Norden B, Chaires JB (1995) J Am Chem Soc 117:4788–4796
21. Linclon P, Broo A, Norden B (1996) J Am Chem Soc 118:2644–2653
22. Greguric I, Aldrich-Wright JR, Collins JG (1997) J Am Chem Soc 119:3621–3622
23. Campisi D, Marii T, Barton JK (1994) Biochemistry 33:4130-4139
24. Hudson BP, Barton JK (1998) J Am Chem Soc 120:6877–6888
25. Brandt P, Norrby T, Akermark B (1998) Inorg Chem 37:4120–4127